



## **BOUNDARY ELEMENT MODELLING OF FRACTAL AND OTHER ENHANCED BANDWIDTH SCHROEDER DIFFUSERS**

Andrew Lock<sup>1</sup> and Damien Holloway<sup>2</sup>

<sup>1</sup>School of Engineering and ICT  
University of Tasmania, Sandy Bay TAS 7005, Australia 1  
Email: [andrew.john.lock@gmail.com](mailto:andrew.john.lock@gmail.com)

<sup>2</sup>School of Engineering and ICT  
University of Tasmania, Sandy Bay TAS 7005, Australia  
Email: [damien.holloway@utas.edu.au](mailto:damien.holloway@utas.edu.au)

### **Abstract**

It is well established that Schroeder diffusers may be used as surface treatment to promote diffuse sound fields in auditoria over a target frequency range. Quadratic Residue Diffusers are very effective within a design frequency bandwidth, and this frequency bandwidth may be significantly extended by a nested or fractal design. Publicly available data typically publishes diffusion coefficients separately for the parent diffuser and the child diffuser, with some ambiguity surrounding the effect the two levels have on each other, and the performance at 'crossover' frequencies. This paper uses an optimised 2D boundary element method to investigate the differences in results when the parent and child diffusers are modelled separately, and as an integrated design. It is found that the scattering properties of the child diffuser are significantly modified by the well of the parent diffuser in which it is placed. More interestingly, the excellent scattering properties of the fractal design may be achieved with only a minor loss of bandwidth using a far simpler and more robust geometry in which the child diffuser is replaced by a concave surface at the base of the well in the parent diffuser. The paper outlines the optimisation of the boundary element code for this task, and compares results for a variety of well bottom shapes with the fractal design.

### **1. Introduction**

An acoustic diffuser is an object or surface profile designed to provide a diffuse reflection from an incident sound wave. While nearly every reflective surface will offer some degree of diffusion, an acoustic diffuser is designed to produce high levels of diffusion or specific diffusion characteristics, often for a design application or frequency range. Diffusion can be either temporal (time-related) or spatial, and is a useful tool in the acoustic treatment of spaces such as critical listening rooms and performance spaces, often to create a more even sound field or to avoid strong reflections [1]. Where traditionally acoustic absorbers have been used to avoid undesirable acoustic effects, there is a growing trend towards the use of diffusers instead [2], and this has increased the need to accurately model their performance.

Schroeder diffusers, named after their creator Manfred Schroeder [3], are popular due to their predictable and desirable diffusion characteristics. While Schroeder diffusers offer high diffusion performance within a design bandwidth, this bandwidth is limited by the practical dimensions of the

diffuser and performance outside the bandwidth limits is poor. Variations to ‘traditional’ Schroeder diffusers including fractal designs (see Section 3.2) are used to increase this design bandwidth while minimising the diffuser’s physical dimensions.

The Boundary Element Method (BEM) is an algorithm derived from Green’s Second Identity used for modelling and analysis of acoustic fields. The BEM is a powerful alternative to Finite Element Analysis (FEA), the Finite-Difference Time Domain (FDTD) and other acoustic modelling techniques, due to the nature of discretisation that effectively reduces the dimensions of the problem by one. The efficient nature of solving acoustic fields using the BEM is particularly suited to problems where the domain is large or considered infinite, such as external diffusion of an object in an incident sound field.

This paper will firstly introduce optimised methods of computing an external diffusion model with the BEM, with particular reference to Schroeder diffusers. The BEM is based on a program initially written by Rocchi [4], which has been developed to achieve significant increases in speed and accuracy through the implementation of advanced discretisation of the diffuser shape and efficient analytic and numeric integrals of terms used in matrix calculations. The paper will then describe Schroeder diffusers and use this optimised BEM code to model performance of ‘traditional’ Schroeder diffusers, fractal diffuser designs and a new diffuser design that offers diffusion performance comparable with fractal designs but with a simpler and more robust geometry.

## 2. Boundary element method development

### 2.1 BEM Theory

Extended derivations of the Boundary Element Method (BEM) may be found in several sources including [5] and [6], a summary will be presented here.

Time periodic acoustic fields may be described in terms of the real part of a velocity potential  $\Phi = \Phi_0 e^{-i\omega t}$  governed by the Helmholtz equation

$$\nabla^2 \Phi + k^2 \Phi = 0, \quad (1)$$

in terms of which velocity  $\mathbf{V}$  and pressure  $p$  are respectively

$$\mathbf{V} = \nabla \Phi, \quad (2)$$

$$p = -\rho \frac{\partial \Phi}{\partial t} = i\rho\omega\Phi. \quad (3)$$

Here  $\rho$  is the density of the acoustic medium,  $k = \frac{2\pi}{\lambda} = \frac{\omega}{c}$  is the wavenumber and  $\lambda$ ,  $\omega$  and  $c$  are respectively the wavelength, angular frequency and speed of sound.

Specific exterior problems are further specified by expressing the total potential as the sum of an incident potential  $\varphi$  (e.g. due to an unconfined sound source, typically a plane, spherical or cylindrical wave) and a scattered (diffracted) wave potential  $\phi$ , both satisfying a radiation condition, and the sum of which satisfies the body surface boundary condition. For a rigid body the latter condition is one of zero normal velocity, hence

$$\nabla \phi \cdot \mathbf{n} = -\nabla \varphi \cdot \mathbf{n} = -\mathbf{V}_I \cdot \mathbf{n} \quad (4)$$

where  $\mathbf{V}_I$  is the incident wave local velocity, and  $\mathbf{n}$  is the unit normal to the body pointing into to the acoustic domain (out of the body).

The BEM solves this by discretising Green’s second identity, derived from the divergence theorem, which may be expressed as

$$\oint (\phi(\mathbf{q}) \nabla G(\mathbf{p}, \mathbf{q}) \cdot \mathbf{n}_q - G(\mathbf{p}, \mathbf{q}) \nabla \phi(\mathbf{q}) \cdot \mathbf{n}_q) dS_q = -C\phi(\mathbf{p}) \quad (5)$$

where  $\mathbf{p}$  is an arbitrary point within the acoustic domain and  $\mathbf{q}$  is a point on the domain boundary and

the integral is evaluated over the entire domain boundary.

Of particular interest is when  $\mathbf{p}$  is on the boundary, in which case a choice suitable for 2D exterior problems of  $G(\mathbf{p}, \mathbf{q}) = \frac{i}{4} H_0^{(1)}(kr)$  (where  $r = |\mathbf{q} - \mathbf{p}|$  and  $H_0^{(1)}(x)$  is the Hankel function of the first kind and order zero [7]) leads to  $C = \frac{1}{2}$ . By dividing the boundary (a closed curve for 2D problems) into discrete small segments bounded by points  $\mathbf{q}_i$ , over which  $\phi$  and  $\nabla\phi$  may for practical purposes be assumed constant and equal to the value at the centroid, this becomes a matrix equation

$$-\frac{1}{2}\{\phi\} = [M]\{\phi\} + [L]\{\mathbf{V}_I \cdot \mathbf{n}\} \quad (6)$$

where

$$L_{ij} = \int_{\mathbf{q}_{j-1}}^{\mathbf{q}_j} G(\mathbf{p}_i, \mathbf{q}) ds_{\mathbf{q}} = \int_{\mathbf{q}_{j-1}}^{\mathbf{q}_j} \frac{i}{4} H_0^{(1)}(kr) ds_{\mathbf{q}}, \quad (7)$$

$$M_{ij} = \int_{\mathbf{q}_{j-1}}^{\mathbf{q}_j} \nabla G(\mathbf{p}_i, \mathbf{q}) \cdot \mathbf{n}_{\mathbf{q}} ds_{\mathbf{q}} = \int_{\mathbf{q}_{j-1}}^{\mathbf{q}_j} \frac{-ik}{4} H_1^{(1)}(kr) \mathbf{r} \cdot \mathbf{n}_{\mathbf{q}} ds_{\mathbf{q}}, \quad \mathbf{r} = \frac{\mathbf{q} - \mathbf{p}_i}{|\mathbf{q} - \mathbf{p}_i|}. \quad (8)$$

The integrals  $L_{ij}$  and  $M_{ij}$  are not in general known in closed form and must be integrated numerically, which is very efficiently accomplished using Gaussian quadrature [7]. The self-influence terms ( $i = j$ ) can however be evaluated analytically, and it is desirable to do so since they contain a singularity at  $r = 0$ . Some authors remove the singular leading term in the Taylor expansion (of order  $\ln r$  or  $\frac{1}{r}$ ) and apply quadrature to the remainder, but using results in [7] it can be shown

$$\int_{-a}^a H_0^{(1)}(kr) dr = 2a H_0^{(1)}(ka) + \pi a \left( \mathbf{H}_0(ka) H_1^{(1)}(ka) - \mathbf{H}_1(ka) H_0^{(1)}(ka) \right), \quad a = \frac{|\mathbf{q}_i - \mathbf{q}_{i-1}|}{2} \quad (9)$$

$$\int_{-a}^a H_1^{(1)}(kr) dr = -\frac{2}{k} H_0^{(1)}(ka). \quad (10)$$

The Hankel function  $H_n^{(1)}(a)$  is easily evaluated using a built-in function in Matlab but the Struve function  $\mathbf{H}_n(a)$  had to be evaluated using a truncated infinite series, thus

$$\int_{-a}^a H_0^{(1)}(kr) dr = \frac{2}{k} \left\{ H_0^{(1)}(ka) \sum_{n=0}^{\infty} s_n + H_1^{(1)}(ka) \sum_{n=0}^{\infty} t_n \right\} \quad (11)$$

where

$$s_0 = ka, \quad s_n = \frac{-(ka)^2}{(2n-1)(2n+1)} s_{n-1}, \quad t_0 = (ka)^2, \quad t_n = \frac{-(ka)^2}{(2n+1)^2} t_{n-1}. \quad (12)$$

These series converged rapidly with appropriate element length relative to wavelength.

## 2.2 BEM optimisation techniques

### 2.2.1 Gaussian quadrature rules

As mentioned above, the integrals of equations (7) and (8) are evaluated using Gaussian quadrature. Integration accuracy could be arbitrarily improved, at a cost, by increasing the order of the integration rule. For line integrals the order of approximation is  $2N - 1$  where  $N$  is the number of integration points (i.e. a 6 point rule is equivalent to fitting an 11<sup>th</sup> order polynomial). Abscissae and weights for  $N=2, 4, 6$  and 10 (amongst others) are published in [7], and a good balance between efficiency and accuracy was found by adapting the integration rule depending on the normalised distance  $r$  of the source point  $\mathbf{q}$  from the collocation point  $\mathbf{p}$  according to the rule in Table 1.

Table 1. Gauss integration points for various source-collocation distances

Source-collocation distance $r/\lambda$	Number of integration points $N$
$< 0.5$	10
$0.5 - 1$	6
$1 - 3$	4
$> 3$	2

### 2.2.2 Self influence terms

As already mentioned,  $G$  and  $\nabla G$  have singularities at  $r = 0$ . Crude results are obtained by using a quadrature rule with even  $N$ , which does not include a point at  $r = 0$  (unlike odd  $N$ , which can't be evaluated at all). Substantially better results are obtained however by numerically integrating the desingularised forms  $\left(H_0^{(1)}(kr) - \frac{2i}{\pi} \ln kr\right)$  and  $\left(H_1^{(1)}(kr) + \frac{2i}{\pi kr}\right)$ , and adding the analytic integrals of  $\frac{2i}{\pi} \ln kr$  and  $\frac{-2i}{\pi kr}$ , which are easily evaluated. But for relatively little additional computational cost (since this is only required for the diagonal elements) the full analytic integration presented in equations (9)–(12) gave accuracy that was significantly better again.

### 2.2.3 Code restructure

The vast majority of run time is spent on computing the [L] and [M] matrices. Optimising the choice of quadrature rule clearly therefore had a big impact on run time, but further significant speed gains were made by restructuring code to minimise recalculation of quantities and/or to exploit Matlab's vector algebra capabilities. On the other hand some Matlab functions, such as dot products of vectors with only two elements, could actually be performed faster by manually programming them.

### 2.2.4 Treatment of sharp edges

A major source of errors is the steep pressure gradient in the vicinity of sharp edges (corners in 2D). Furthermore, the coefficient  $C$  in equation (5) at the corner is not  $\frac{1}{2}$ , but for an edge angle of  $\theta$  is actually  $\theta/2\pi$  (hence  $\frac{1}{2}$  for a smooth boundary, and it is noted that in the present BEM formulation the boundary condition is applied at the element mid-point, which is never a corner). Nevertheless this contributes to the abrupt change of  $\phi$  (or pressure) near the edge.

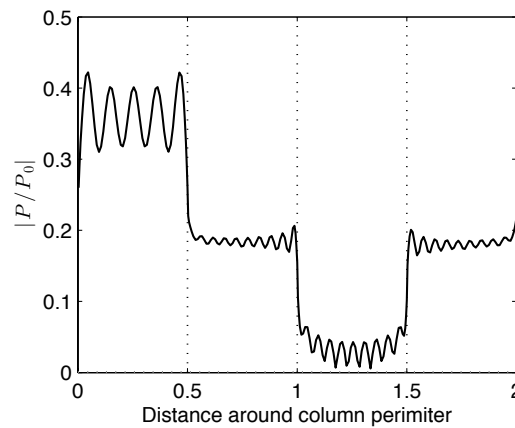


Figure 1. Surface pressure around an infinitely long 0.5 m×0.5 m square column due to a cylindrical point source at 3240 Hz. The horizontal axis represents distance around the perimeter, with edges at 0, 0.5, 1.0, 1.5 and 2.0 m. 0–0.5 m is the side facing the source.

The steep pressure gradient at the edges is clearly visible in Figure 1, showing a typical surface

pressure around a square object. It would not be a problem for shapes defined by smooth curves, but is critical for modelling any object with edges, and similar results were found with the Schroeder diffusers.

A twofold approach has been adopted to maintain accuracy. First, a 20 point quadrature rule was used on all elements attached to an edge. Second, the element size was refined approaching edges. Elements were reduced to  $\frac{1}{3}$  times the global size at the corners, and transitioned in a geometric progression over 5 elements, thus adjacent elements did not differ by more than a ratio of  $3^{0.2} = 1.25$ . A substantial improvement in accuracy for a given number of elements was found from adopting both of these techniques, as discussed below. The authors plan to investigate this further in future work.

### 2.2.5 Singular frequencies

At particular frequencies corresponding to the eigen values of equation (6) the problem becomes poorly conditioned and accuracy substantially declines. This was solved by placing an additional boundary inside the diffuser body, creating a second acoustic domain entirely independent of the primary domain. As this domain is not connected to the primary domain, and all boundary and field conditions are enforced in both domains, it had no effect on the solution other than to change the eigen frequencies, hence to remove the singularity at the problem frequencies and vastly improve accuracy. Of course new problem frequencies are thus introduced, but the solution without the additional secondary domain is perfectly suitable for these frequencies.

### 2.2.6 Future work

For the problem to be well conditioned, the element size on any thin panels (such as those separating the diffuser wells) had to be smaller than the panel thickness. This was quite restrictive. Wu [8] has published a ‘thin panel’ BEM formulation that overcomes this problem. This represents the panel as a single surface so would not only allow larger elements, but would halve the number of elements on the panels (though with two equations for each).

Further gains could also be made by use of a higher order formulation, in which  $\phi$  and  $\nabla\phi$  may vary linearly on each element, thus  $\phi$  would be defined at element end points and would vary continuously around the boundary. This would be of benefit at corners in particular.

## 2.3 BEM Validation and Improvement Quantification

Initial validation of the optimised BEM code was performed for the case of an infinite cylinder in a plane wave acoustic field, for which there exist published solutions by Morse & Ingard [9], Kuyama [10] and Wiener [11]. The maximum deviation between a diffusion result from the BEM and analytic solution published by Morse & Ingard [9] was less than 0.003% for a cylinder of radius  $a = \frac{1}{k}$  and observation radius  $r = \frac{2}{k}$ . The BEM code was further validated for the more challenging case of a QRD with the effects of thin panels and sharp corners, including comparisons between results gained using alternative methods such as the commercial Finite Element program ANSYS. Further information on the BEM code validation can be found in Lock [6].

Figure 2 shows a comparison between the BEM code published by Rocchi [4] and the BEM code developed in this work. The optimisations described above produced more than 240 times increase in solution speed while maintaining or even improving accuracy. The lower half of Figure 2 shows that for the test case at least 400 elements are required in the fully optimised code with edge refinement for reasonable convergence of results, requiring 0.25 minutes (15 sec) to solve. Without edge refinement more than 1000 elements are required for the same accuracy, and the solution time is increased to more than 1 minute. Without any optimisation 1000 elements took about 60 minutes.

## 3. Diffuser design

### 3.1 Schroeder Diffusers

Manfred Schroeder is considered to have made the most substantial breakthrough in diffuser design in

1975, when he presented his theory of reflection phase grating diffusers [3],[12]. Schroeder diffusers offered a key advantage in that their performance could easily be predicted, and they are still considered amongst some of the most effective diffuser designs used today.

A key feature of phase grating diffusers are regions of high sound pressure reflected in radial directions from the diffuser, named ‘diffusion lobes’ most prominent at multiples of the design frequency. These diffusion lobes give Schroeder diffusers their high diffusion properties.

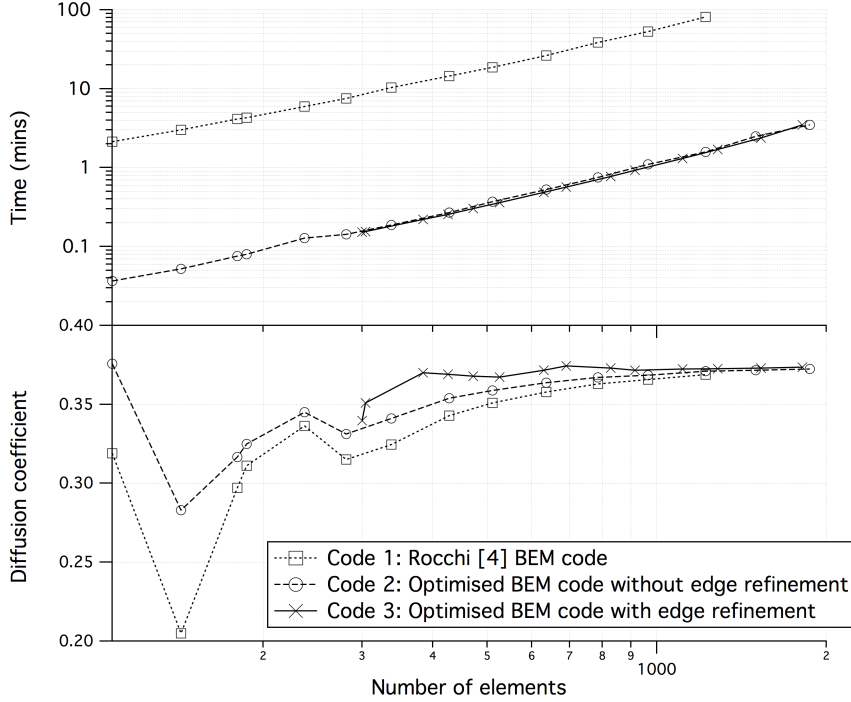


Figure 2: Comparison of solution time and convergence from 3 BEM code versions. Three repeating periods of an  $N = 7$  QRD,  $Nw_T = 0.56$  m,  $f = 2000$  Hz =  $4f_0$  (symbols defined in Section 3.1).

In two dimensions, Schroeder phase grating diffusers consist of wells of even width and varying depth separated by thin panels. Different mathematical patterns govern the depth of successive wells, and installations most commonly consist of multiple repeated periods of the chosen pattern. A period consists of  $N$  wells of width  $w$ , separated by a thin panel of width  $w_p$ . The total width of a well and panel is represented by  $w_T$ , and consequently the period width is written as  $Nw_T$ , shown in Figure 3.

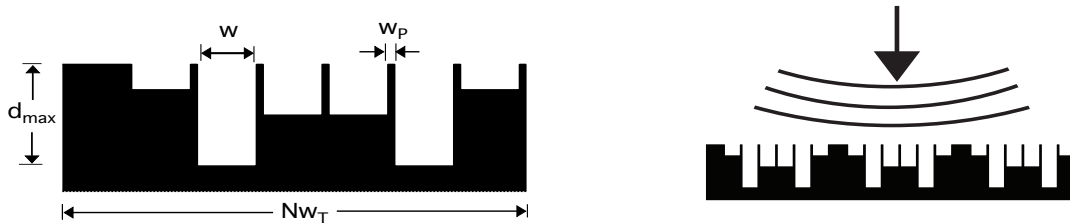


Figure 3. (Left) One period of a QRD; (Right) Repeating periods of a QRD array.

### 3.1.1 Quadratic Residue Diffusers

The most popular Schroeder diffuser is the Quadratic Residue Diffuser (QRD), named after the pseudo-random Quadratic Residue Sequence as first studied by Gauss and Legendre [3], which dictates successive relative well depths. The  $n^{\text{th}}$  term in the sequence,  $s_n$ , is defined as

$$s_n = n^2 \text{ modulo}(N),$$

where  $n = 0, 1, 2 \dots (N - 1)$ , and  $\text{modulo}(N)$  represents the least non-negative remainder when divided by  $N$ . The value  $N$  is restricted to prime numbers, and also represents the number of terms in each repeating sequence. The depth  $d_n$  of the  $n^{\text{th}}$  well in a quadratic residue diffuser for a design frequency of  $f_0$  and prime number  $N$  are determined from the equation

$$d_n = \frac{cS_n}{2Nf_0}, \quad (13)$$

where  $c$  is the speed of sound in air.

### 3.1.2 Design frequency limitations

A design principle behind Schroeder's theory of phase grating diffusers is that longitudinal wave propagation within the wells dominates transverse waves. From this, the upper frequency limit to the applicability of this theory can be stated as

$$\frac{\lambda_{\min}}{2} = w. \quad (14)$$

Another limiting factor of QRDs is the period width,  $Nw_T$ . While even energy lobes can be expected at the design frequency,  $f_0$ , if the period width is too small only one energy lobe is present in the specular reflection direction, and the diffuser displays poor diffusion characteristics [2].

The effective bandwidth of a simple QRD can therefore be predicted as

$$f_{\min} = f_0 = \frac{cS_{\max}}{2Nd_{\max}}, \quad (15)$$

provided that  $Nw_T > \lambda_0$ , and

$$f_{\max} = \frac{c}{2w}. \quad (16)$$

## 3.2 High bandwidth diffusers

As shown in the previous section, each diffuser design has an effective working range. In order to extend that range, nested or fractal designs may be used [13]. Typically a 'child' QRD is placed in the bottom of each well of a parent QRD. For a diffuser of period  $N$  the child QRD will be approximately  $N$  times smaller than the parent (though this is not necessarily the case for the well depth). The performance of the parent and child are generally published separately by manufacturers. However the child diffuser scatters sound within a confined space (the well), so its performance may potentially differ significantly from its published unconfined performance. Furthermore, there may be simpler geometries that produce good scattering of high frequency sound within a well.

It is of interest to determine what if any interaction there is between parent and child that may enhance or degrade performance, and to further investigate alternative geometries. This paper therefore investigates the following four diffuser designs:

1. The *parent QRD* is an  $N = 7$  QRD of period width  $(Nw_T)_{\text{parent}} = 0.85$  m and design frequency  $f_{0,\text{parent}} = 400$  Hz.
2. The *child QRD* is an  $N = 7$  QRD approximately a  $\frac{1}{7}$  scale of the parent QRD, with  $(Nw_T)_{\text{child}} = w_{\text{parent}} = 10.93$  cm and  $f_{0,\text{child}} = 7f_{0,\text{parent}} = 2800$  Hz.
3. The *fractal diffuser* is the parent QRD with a child QRD diffuser at the bottom of each well.
4. The *QRD with nested concave* is the parent diffuser with a concave surface at the bottom of each well. The concave curve follows a quadratic profile with a maximum deviation of  $1.35$  cm  $= \frac{w}{8}$ .

An array of 5 repeating periods was modelled for each diffuser design, with the exception of the child QRD for which an array of 35 periods was modelled. Each diffuser design is shown in Figure 4.

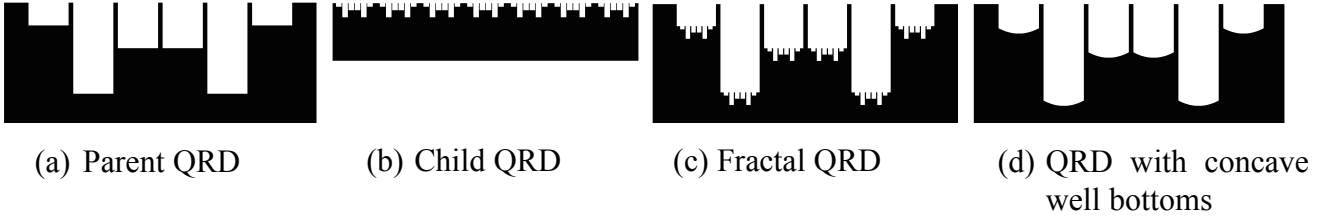


Figure 4: Diagram of each diffuser modelled. 1 period of (a), (c), (d); 7 periods of (b).

### 3.3 Test Details

Each diffuser was modelled with a single cylindrical source at normal ( $0^\circ$ ) incidence at a distance of 20 m. Diffusion coefficients were based on sound pressures at 360 receivers on a semicircle of 10 m radius, and 7 logarithmically spaced frequencies in each  $1/3$  octave bandwidth, in accordance with ISO 17497-2 [14]. The panel thickness relative to well width was  $\frac{w_P}{w_T} = 0.1$ .

An accuracy study suggests the results in this paper are accurate to within  $\pm 2\%$  below 3 kHz, and within  $\pm 4\%$  between 3 kHz and 10 kHz [6]. Accuracy was reduced with a source location at incident angles to the diffuser, and therefore in this investigation the model was limited to source location at an angle  $\theta = 0^\circ$  to the centre of the diffuser. The reduced accuracy observed at incident angles can be explained from the thin panel effect as described by Cox and D'Antonio [2] and mentioned in Section 2.2.6. The implementation of the BEM thin panel solution as published by Wu [8] may resolve these errors, but will result in a model where thin panels are considered to have infinitely small thickness, and at high frequencies the model may not accurately represent the physical diffuser.

## 4. Results

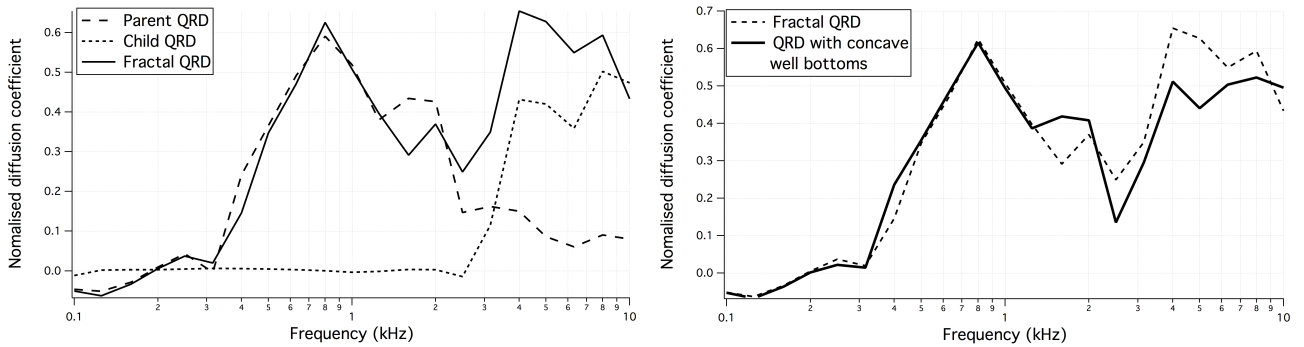


Figure 5: (Left) Normalised diffusion coefficient of a parent, child, and corresponding fractal QRD; (Right) Normalised diffusion coefficient of a fractal QRD and QRD with nested concave wells.

Figure 5 shows the normalised diffusion coefficient (defined above) for the four diffuser designs tested for the frequency range between 100 Hz – 10 kHz. Of particular interest is the comparative performance of each diffuser design at the crossover frequencies between 1.5 – 4 kHz, and at high frequencies above 4 kHz. The diffusion polar pattern for each diffuser at 4 kHz is shown in Figure 6, at which frequency there are substantial differences in the performance of all four diffuser designs. Pressures shown in Figure 6 are scaled with respect to the maximum receiver pressure for each design.

Complex geometries, such as the fractal QRD, required over 5000 elements to obtain an accurate solution at high frequencies, and obtaining the results in Figure 5 required a solution at 147 frequencies for each the diffuser and a reference flat plate used to normalise the diffusion coefficient. For the case of a detailed diffuser such as a fractal QRD, a full set of results between 100 Hz – 10 kHz required approximately 12 hours to compute.

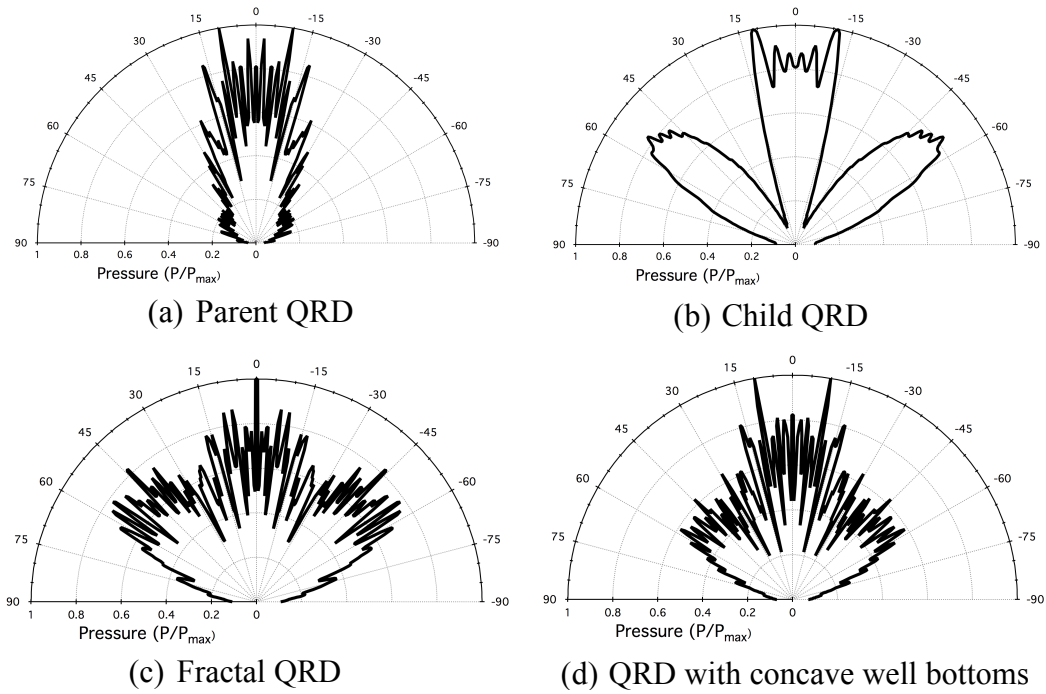


Figure 6. Polar plot example of the four tested diffuser designs at  $f = 4000 \text{ Hz}$ . Normalised diffusion coefficients are (a) = 0.15, (b) = 0.43, (c) = 0.65, and (d) = 0.51.

## 5. Discussion

From Figure 5 it is observed that the fractal diffuser offers slightly inferior performance when compared to the corresponding parent QRD at frequencies at which half the wavelength is comparable to the well width, or the ‘crossover’ frequencies (i.e. around 1500 Hz). One explanation for this is the effect of the nested child diffuser on the quadratic residue sequence interference pattern, resulting in reduced energy lobe behaviour. The reduction in performance at the crossover frequencies is offset by increased performance at high frequencies, where the fractal diffuser offers far superior diffusion to the parent or child diffuser when modelled individually. The superior high frequency performance and extended bandwidth is consistent with previous findings by Cox & D’Antonio [2].

Figure 6 shows that at the top end of the crossover frequency band the difference in scattering behaviour is much more profound than is suggested by the diffusion coefficient alone. In particular, the reasonably good diffusion coefficient of the Child QRD hides the fact that there is significant lobing. In contrast both the Fractal and Concave QRD are show far better diffusion, with relatively uniform pressures over around  $120^\circ$ . Interestingly the specular reflection peak evident in the Fractal QRD is replaced with two individual peaks at around  $\pm 10^\circ$  in the Concave QRD.

The novel concave diffuser design modelled in this work shows almost identical performance to the parent diffuser until the upper limit of the parent diffuser design bandwidth (around 2 kHz). At frequencies at which the wavelength is smaller than the well width, the concave diffuser design offers a level of performance comparable with the fractal diffuser and superior to the child diffuser. While the performance of the concave diffuser may be considered slightly worse at mid-high frequencies than the fractal diffuser, the simplicity of design offers advantages including robustness, reduced production cost, and decreased risk of absorption. Fujiwara & Miyajima recorded absorption coefficients between 0.3 and 1 for QRDs [15], which was later attributed to poor build quality and bonding of the tested diffusers [16]. The simplicity of the concave QRD design in this work offers a clear advantage in reducing the risk of high absorption. It is likely that optimisation of the concave curve profile incorporated in the diffuser may further improve the high frequency diffusion performance.

## 5. Conclusion

This investigation developed an optimised implementation of the BEM to model external diffusion from

Schroeder diffusers. Increases in speed and accuracy gained from advanced discretisation of the diffuser shape and analytic integration of diagonal matrix elements, amongst other developments, allowed for modelling of geometries with greater levels of detail including large arrays of small QRDs, fractal QRDs, and a novel QRD design with concave well bottoms.

The diffusion performance of a fractal QRD was compared to the corresponding parent QRD, child QRD and QRD with concave well bottoms. Key findings from the results include:

- The performance of the child QRD is modified, and generally enhanced, by being incorporated within a fractal QRD;
- The fractal QRD exhibited strong performance over a wide frequency band, but there is a crossover frequency band where performance is reduced by about 50%;
- A novel QRD design with concave well bottoms introduced in this investigation has slightly different characteristics at the crossover frequency band, but is generally speaking comparable to the fractal QRD design and incorporates a far simpler and more robust design; and
- There is scope to optimise the curve profile of the QRD with concave well bottoms, which is likely to further improve performance.

## Acknowledgements

The authors are grateful to Luca Rocchi, who wrote the original BEM code that has been developed for this work.

## References

- [1] Everest, F.A. and Pohlmann, K.C. *Master Handbook of Acoustics*, 5<sup>th</sup> edition, McGraw-Hill, 2009.
- [2] Cox, T. and D'Antonio, P. *Acoustic Absorbers and Diffusers: theory design and application*, CRC Press 2009.
- [3] Schroeder, M.R. "Diffuse sound reflection by maximum-length sequences", *The Journal of the Acoustical Society of America*, **57**(1):149–150, (1975).
- [4] Rocchi, L. *Quadratic residue diffusers: Modelling through the boundary element method*. BE(Hons) Thesis, University of Tasmania, 2014.
- [5] Kirkup S. *The boundary element method in acoustics*. Integrated sound software, Heptonstall 1998
- [6] Lock, A. *Development of a 2D boundary element method to model Schroeder acoustic diffusers*, BE(Hons) Thesis University of Tasmania, 2014.
- [7] Abramowitz, M. and Stegun, I.A. *Handbook of Mathematical Functions with formulas, graphs and mathematical tables*. Applied Mathematics Series 55, National Bureau of Standards, 1964
- [8] Wu, T.W. "A direct boundary element method for acoustic radiation and scattering from mixed regular and thin bodies". *Journal of the Acoustical Society of America*, **97**(1): 84–91, (1995).
- [9] Morse P.M. and Ingard, K.U. *Theoretical acoustics*. Princeton University Press, 1986
- [10] Kuyama, T. "Some calculated results of the diffraction of sound waves by a cylindrical obstacle". *Proceedings of the Physico-Mathematical Society of Japan*, **15**, 366–370, (1933).
- [11] Wiener, F.M. "Sound diffraction by rigid spheres and circular cylinders", *The Journal of the Acoustical Society of America* **19**(3), 444–451, (1947).
- [12] Schroeder, M.R. "Binaural dissimilarity and optimum ceilings for concert halls: More lateral sound diffusion", *The Journal of the Acoustical Society of America*, **65**(4), 958–963, (1979).
- [13] D'Antonio, P. and Konnert, J. "The QRD diffractal: a new one- or two-dimensional fractal sound diffuser", *Journal of the Audio Engineering Society*, **40**(3), 117–129, (1992).
- [14] ISO 17497-2:2012 Acoustics – sound-scattering properties of surfaces Part 2: Measurement of the directional diffusion coefficient in a free field, *International Organization for Standardization*, Geneva, Switzerland, 2012.
- [15] Fujiwara, K. and Miyajima, T. "Absorption characteristics of a practically constructed Schroeder diffuser of quadratic-residue type", *Applied Acoustics*, **35**(2), 149–152, (1992).
- [16] Fujiwara, K. "A study on the sound absorption of a quadratic-residue type diffuser", *Acta Acustica united with Acustica*, **81**(4), 370–378, (1995).